Dynamic Performance of Model Rocking Footings on Sand Reinforced by Soil-Cement Columns

Jeffrey T. Newgard, P.E.[1], Tara Hutchinson, Ph.D., M.ASCE[2], John S. McCartney, Ph.D., P.E., F.ASCE[2]

[1] Department of Structural Engineering, University of California-San Diego, 9500 Gilman Drive, San Diego, CA 92093-0085; e-mail: jnewgard@eng.ucsd.edu, jthomasnewgard@gmail.com
[2] Department of Structural Engineering, University of California-San Diego, 9500 Gilman Drive, San Diego, CA 92093-0085; e-mail: tahutchinson@eng.ucsd.edu
[3] Department of Structural Engineering, University of California-San Diego, 9500 Gilman Drive, San Diego, CA 92093-0085; e-mail: mccartney@ucsd.edu

ABSTRACT

This study focuses on the load-deformation response of a heavily loaded rocking footing on sand reinforced by soil-cement columns via centrifuge-model scale shake table tests. In a previous study involving the same footing on unimproved ground, the footing exhibited overturning failure and excessive settlement. To mitigate this, the present study aims to control the kinematics of the footing via strategic ground improvement while maintaining the enhanced energy dissipation characteristic of a rocking footing. The ground improvement technique consists of soil-cement mixed columns which were cast externally and then placed in the model sand layer during pluviation. Shake sequences are applied to both determine the frequency response of the soil-structure system as well as to induce controlled yielding in the improved soil. The addition of paired soil-cement columns at the ends of the footing was found to significantly reduce settlement during rocking and preserve re-centering throughout demanding shaking events.

INTRODUCTION

Rocking footings dissipate energy into foundation soils and thereby reduce damage to superstructure elements (e.g., Deng et al. 2012, Sharma et al. 2020). Additionally, they have a natural tendency to re-center themselves under the pull of gravity as they rock about their corners (Housner, 1963). However, to induce rocking, they must be sized smaller than a more typical stiff, elastic footing and thus have a slimmer margin in terms of the factor of safety for bearing capacity and further are prone to excessive settlement. Physical experiments conducted by Khosravi et al. (2019) and Anastasopoulos et al. (2012), in which soil-cement grids were mixed

and dense crust was compacted beneath the footing, and numerical studies conducted by Liu & Hutchinson (2018), in which stone columns were arranged in varying geometries beneath the footing, all demonstrated how ground improvement can mitigate such detrimental kinematics. Despite these studies, there is a need for a wider variety of ground improvement techniques to be investigated as few of the tests in the Foundation Rocking, Dynamic Loading (FoRDy) database (Gavras et al. 2020) incorporate ground improvement. They could inform additional ground-improvement specific provisions in existing design code for rocking footings (ASCE 41-17). By expanding the database of tests demonstrating the beneficial aspects of rocking footings and the potential for ground improvement to control detrimental aspects, geotechnical engineers can move forward with more confidence implementing this type of design into foundation engineering practice.

TEST CONFIGURATION

The model soil conditions, footing geometry and loading, and test equipment and instrumentation are all described in detail in Newgard et al. (2022). A centrifuge g-level of N = 25 was adopted in this study. Ottawa F-65 sand was pluviated through a pair of sieves (No. 8 and No. 12) to disperse the sand uniformly, resulting in deposits with relative density of about 50% when the drop height was minimized. At this medium dense state, the sand was expected to settle excessively under the weight of a heavily loaded rocking footing and thus be a strong candidate for ground improvement.

The soil-cement columns were cast externally in 25 mm (1 in.) diameter molds following procedures in the FHWA Deep Mixing Design Manual (Bruce et al. 2012) and then placed in the sand layer during pluviation. The sand surface was sprayed with WD-40 to give it a light cohesion, both to permit excavation of the sand to place the columns, and to prevent sand from unnaturally filling the gaps beneath the uplifting footing during rocking. No structural connection exists between the footing and soil-cement columns. Pictures of the instrumented footing and soil-cement columns are shown in Figure 1, and a schematic of the instrumented footing is shown in Figure 2.

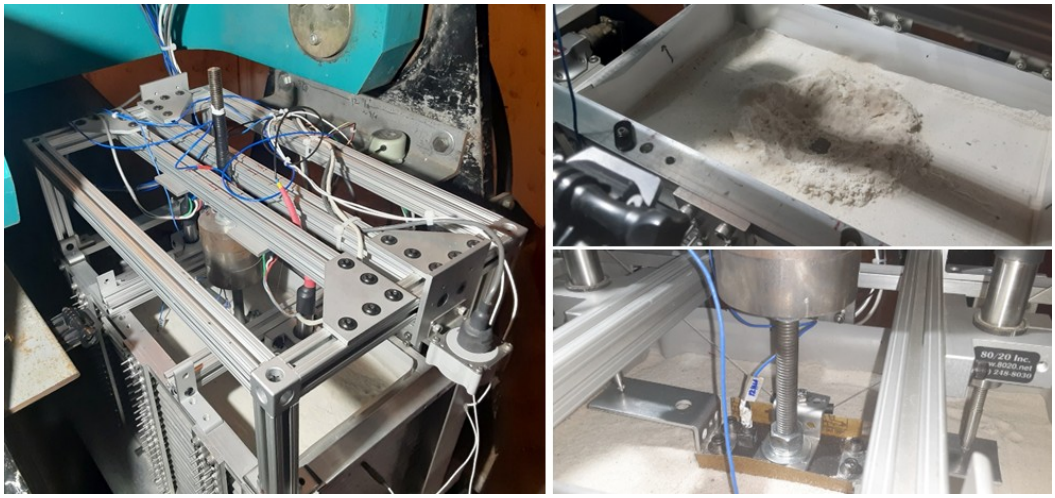

Figure 1. Picture of model footing, installed soil-cement column, and instrumentation within the UCSD geotechnical centrifuge.

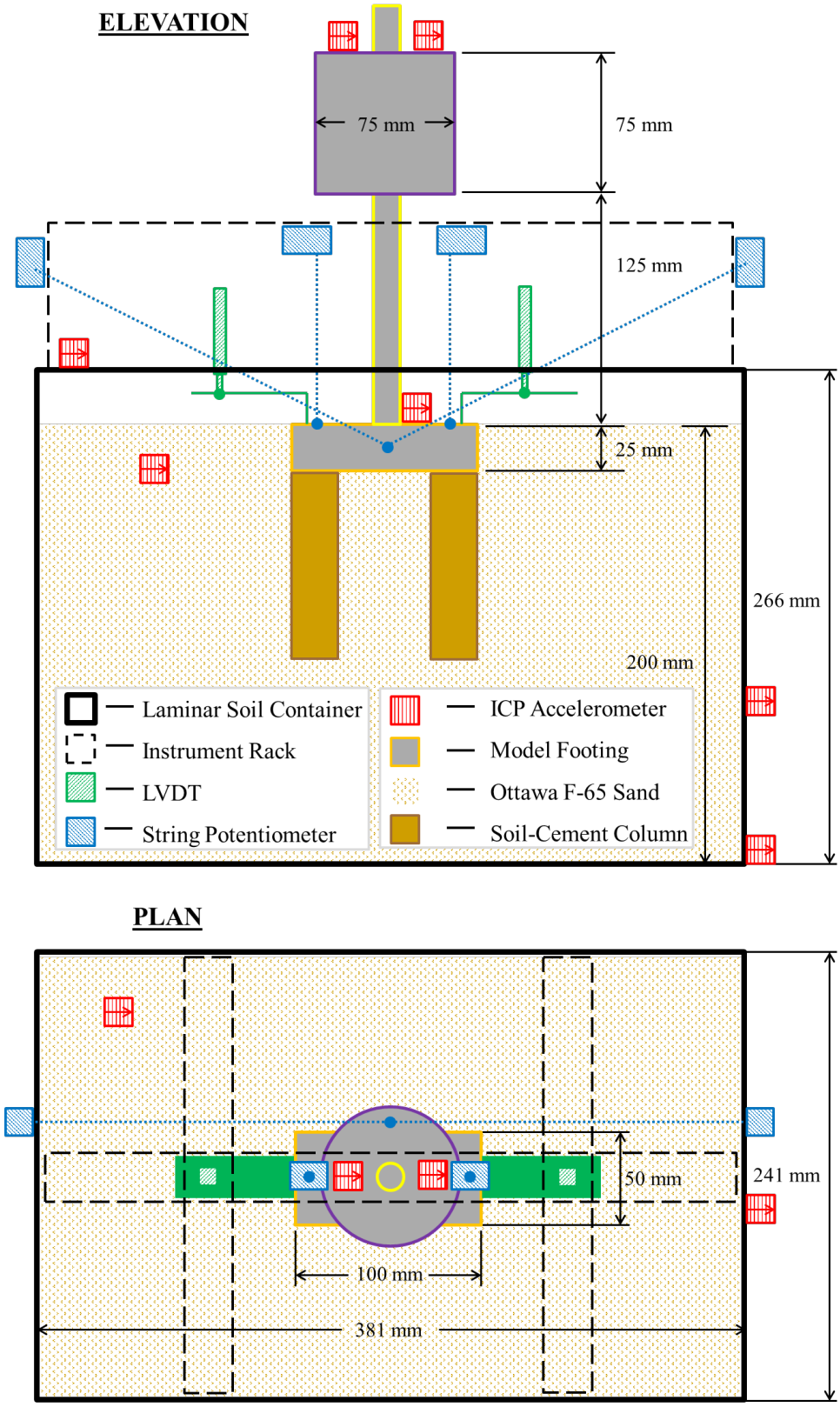

Figure 2. Schematic of model footing and instrumentation. All model scale units.

SOIL-CEMENT COLUMN MIX DESIGN

A well-graded (SW) sand, previously characterized by Zheng et al. (2019), was used for the soil-cement columns after it was observed that preliminary soil-cement columns formed from uniform Ottawa F-65 sand tended to segregate easily and exhibited low compressive strength. A water:binder (w:b) ratio of 2.5 was selected to target an unconfined compressive strength of approximately 1725 kPa (250 psi), following the trendline for a variety of lab-mixed soil-cement columns in Figure 29 of the FHWA Deep Mixing Design Manual. This is the strength required to prevent crushing of a column, derived from a simple moment equilibrium equation where the column is placed at the edge of a footing rocking about its opposite corner. To define the mix design, the mass of binder per soil volume (α) was taken as 200 kg/m^3, the same amount reported in a case history by Arora et al. (2012) where soil-cement mixing was employed at a sandy site to mitigate scour and support shallow foundations. The calculation procedure for the mix design then proceeded as follows:

$$D_R = \frac{\gamma_{d,soil} - \gamma_{d,min}}{\gamma_{d,max} - \gamma_{d,min}} \tag{1}$$

$$\gamma_{d,slurry} = \frac{G_b \gamma_w}{1 + (w:b) G_b} \tag{2}$$

$$\alpha = \frac{w_b}{V_{soil}} \tag{3}$$

$$VR = \frac{V_{slurry}}{V_{soil}} = \frac{\alpha}{\gamma_{d,slurry}} \tag{4}$$

where $\gamma_{d,soil}$ = soil dry unit weight, $\gamma_{d,min}$ = soil minimum dry unit weight, $\gamma_{d,max}$ = soil maximum dry unit weight, D_R = soil relative density, G_b = binder specific gravity, γ_w = unit weight of water, w:b = water:binder ratio, $\gamma_{d,slurry}$ = slurry dry unit weight, w_b = weight of binder, V_{soil} = volume of soil, α = weight ratio of binder:soil, and VR = volume ratio of binder:soil. Once the volume ratio is established, the quantities of soil, binder, and water are determined:

$$V_{mixture} = (No.\,specimens)(Mold\ Volume)(1.2) \tag{5}$$

$$\gamma_{soil} = \gamma_{d,soil} \tag{6}$$

$$w_{soil} = \frac{1}{1 + VR} V_{mixture} \gamma_{soil} \tag{7}$$

$$w_b = \frac{VR}{1 + VR} V_{mixture} \gamma_{d,slurry} \tag{8}$$

$$w_{w,\,slurry} = (w:b)(w_b) \tag{9}$$

$$VR = \frac{\gamma_{soil}}{\gamma_{d,\,slurry}} \frac{w_b}{w_{soil}} \tag{10}$$

where $V_{mixture}$ = volume of entire mixture, γ_{soil} = total unit weight of sampled soil (identical to dry soil used in the lab), w_{soil} = weight of soil, w_{binder} = weight of binder, and $w_{w,slurry}$ = weight of water in slurry. The input parameters and calculated results for the mix design of the soil-cement columns following the above procedure are shown in Table 1 and Table 2, respectively.

Table 1. Inputs and results for soil-cement column mix design.

Parameter	Quantity
Soil Minimum Dry Unit Weight ($\gamma_{d,min}$)	14.19 kN/m^3
Soil Maximum Dry Unit Weight ($\gamma_{d,max}$)	17.26 kN/m^3
Soil Relative Density (D_R)	50%
Binder Specific Gravity (G_b)	3.15
Water:Binder Ratio (w:b)	2.5
Weight Ratio of Binder:Soil (α)	1.96 kN/m^3 (200 kg/m^3)
Number of Specimens	20
Mold Volume	52 cm^3
Achieved Soil Dry Unit Weight ($\gamma_{d,soil}$)	15.73 kN/m^3
Slurry Dry Unit Weight ($\gamma_{d,slurry}$)	3.48 kN/m^3
Volume Ratio of Binder:Soil (VR)	0.56
Volume of Entire Mixture ($V_{mixture}$)	1240 cm^3
Weight of Soil (w_{soil})	1.27 kg
Weight of Binder (w_b)	0.16 kg
Weight of Water in Slurry ($w_{w,slurry}$)	0.40 kg

SOIL-CEMENT COLUMN STRENGTH TESTING

Unconfined compression strength tests were performed on soil-cement columns mixed with both Ottawa F-65 sand and the SW sand. The specimens measured 50 mm (2 in.) in diameter and 100 mm (4 in.) in length and were tested after curing for at least 14 days. The results of these tests are shown in Figure 3. A picture of one of the SW sand columns is also shown in Figure 3. The strength of both batches was less than the target compressive strength of 1725 kPa (250 psi), but because this target was calculated conservatively (neglecting any support from surrounding soil

and treating the columns as an isolated reaction in the moment equilibrium), the SW sand columns were deemed sufficient for use in the centrifuge tests. Future batches could reduce the w:b ratio further although eventually it would become less practical to mix columns at low water contents in a field application.

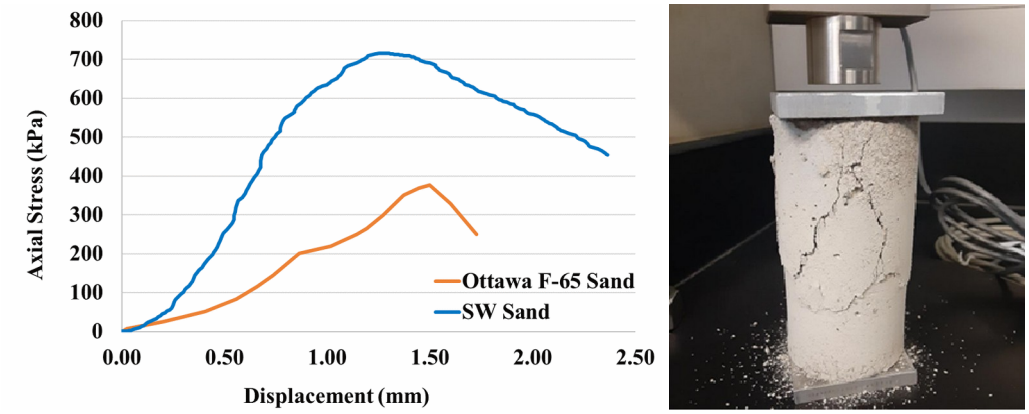

Figure 3. Unconfined compression test results for soil-cement columns and SW sand column following unconfined compression testing.

SHAKE TABLE MOTION

An identical series of shakes was applied to both the unimproved and improved cases for ease of comparison of the results. The shakes were consistent with the ideology of FEMA 461 in which low-level shakes designed to identify the natural frequency of the structure were followed by shakes of increasing magnitude designed to cause greater and greater damage, or in this case yielding of the foundation soils. A summary of the full shake sequence is shown in Table 2.

Table 2. Shake sequence.

Shake Event	Duration[1] (s)	Stimulus Amplitude[1] (V)	Frequency Content[1]
1	0.5	0.07	White Noise
2	0.5	0.10	White Noise
3	0.5	0.15	White Noise
4	0.8	0.10	“Broadband”
5	0.8	0.20	“Broadband”
6	0.8	0.30	“Broadband”
7	0.8	0.40	“Broadband”
8	0.8	0.50	“Broadband”

9	0.8	0.60	“Broadband”
10	0.8	0.70	30 Hz Harmonic
11	0.5	0.15	White Noise

[1] Event characteristics are shown in model scale as they are input to the shake table control program. The Stimulus Amplitude matches the LVDT output (V) mounted to the shake table providing position feedback control.

The movement of the shake table for each event in this sequence is shown in Figure 4. The white noise shakes (Events 1-3) identified a strong tendency of the footing to rock at about 30 Hz. (Note that at N = 25 this corresponds to a natural period of the prototype structure of about 0.8 seconds.) This was consistent with the natural frequency derived from soil-structure interaction procedures in Veletsos and Meek (1974) and Gazetas (1991). Subsequently, the sine sweep comprising the "Broadband" shakes (Events 4-9) was developed such that its response spectrum peaked at this frequency to encourage stronger rocking of the footing. These shakes were followed by a very demanding, long duration 30 Hz harmonic wave (Event 10) and finally another white noise shake (Event 11) to characterize damage to the soil-structure system. It was observed that the rocking footing induced yielding in the foundation soils (i.e., they reached their moment capacity) by about Events 7-8. By performing discrete shakes of increasing magnitude, a sense can be gained of the footing's ability to re-center itself following seismic events of varying intensity.

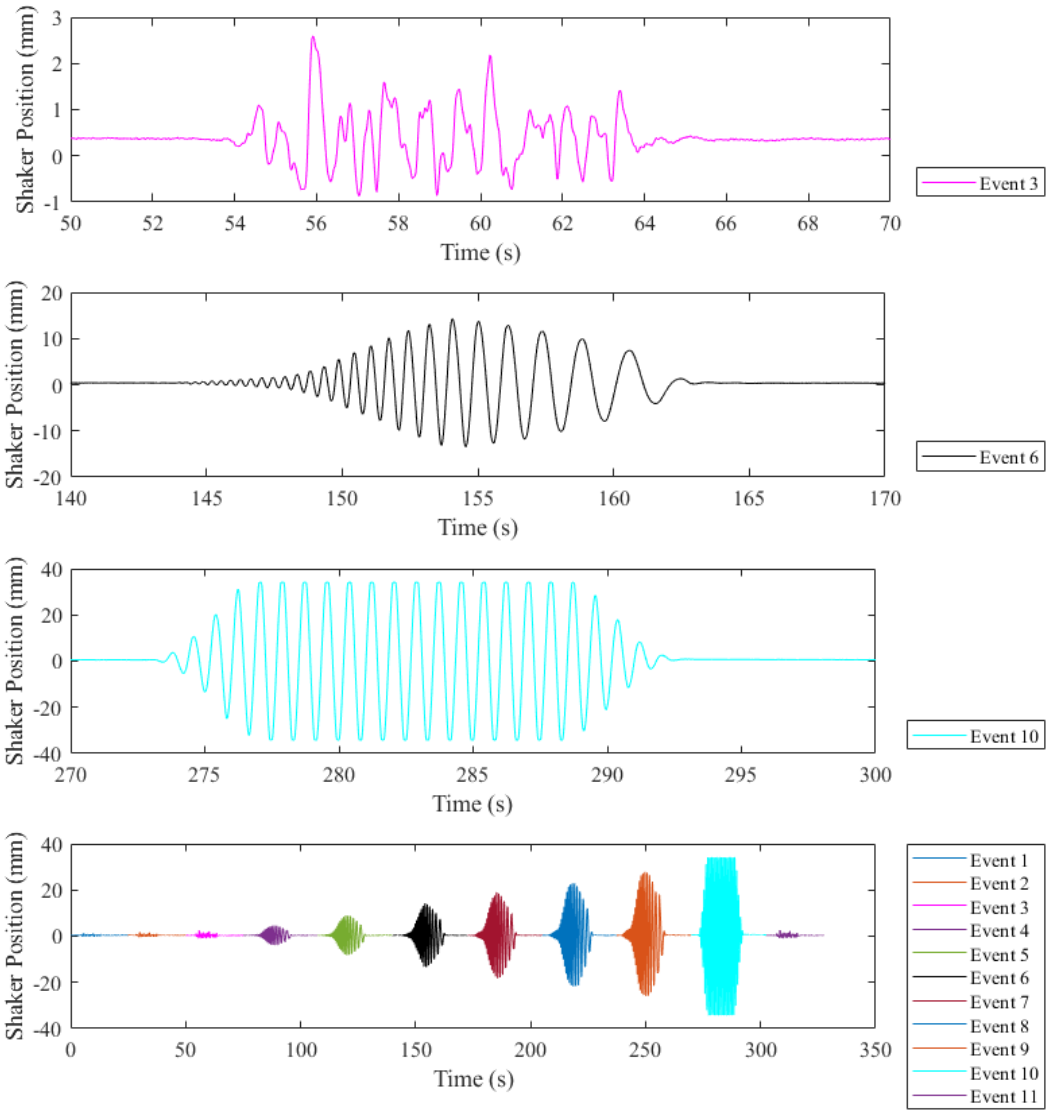

Figure 4. Measured base input motions from the UCSD centrifuge shake table.

DISCUSSION OF RESULTS

This paper presents results from just two select tests, one unimproved case and another with a pair of soil-cement columns placed at each end of the footing about its rocking axis. The columns measure 0.65 m in diameter and 2.50 m in depth, while the footing measures 2.50 m in length, 1.25 m in width, and is embedded 0.65 m beneath the soil surface (all prototype dimensions). The unimproved rocking footing behavior in moment-rotation and settlement-rotation for Shake Events 3-8 are shown in Figure 5a-5f, respectively. The black dashed lines on each of the plots signify the foundation soil's moment capacity, and the blue dashed lines signify the footing's rocking stiffness (see Gajan & Kutter 2008; Deng & Kutter 2012). As expected, the rate of accumulation of settlement increases rapidly once the soil reaches its moment capacity during Shake Event 6 (Figure 5d) and beyond. While the measured rocking stiffness matches the calculated stiffness up to this point, it too experiences a degradation of about 20% following Shake Event 6. The settlements reached in these later events would be beyond any serviceability criterion.

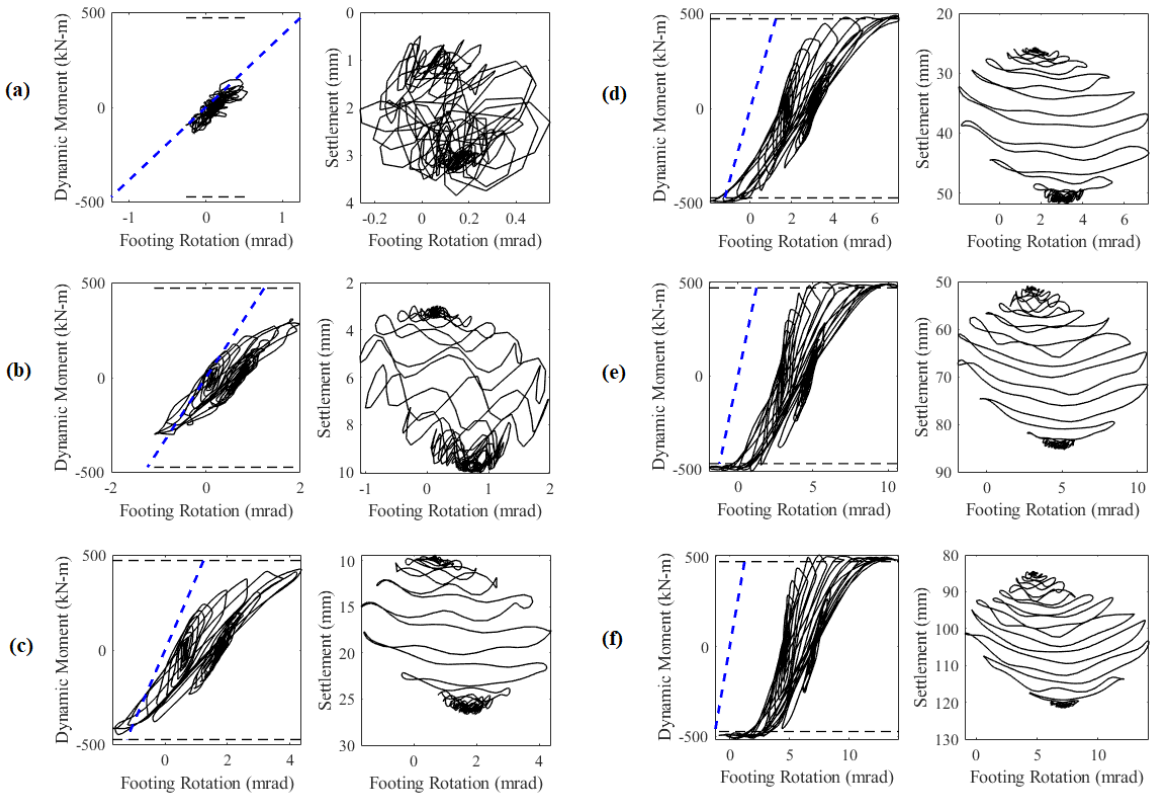

Figure 5. Rocking footing behavior in the unimproved case for Shake Events 3-8 (a-f).

A comparison of the unimproved and improved cases is shown in Figure 6. The residual

settlement (w_r) of the footing normalized by its length (L_f) as well as the re-centering ratio (defined as the ratio between the maximum rotation during the shake and the residual rotation following the shake, when the footing is unloaded) are plotted against cumulative rotation (see Sharma & Deng 2020). The two cases from the present study are compared to curves for a similarly loaded unimproved footing from Deng et al. 2012. Note that the re-centering ratio from this previous study is reported at a single cumulative rotation reached during their tests. These two unimproved cases match well for both metrics lending confidence in the results. The paired soil-cement columns reduce the rate of accumulated settlement by more than 50%, and even as the cumulative rotation increases (i.e., seismic demand becomes greater), the footing continues to re-center itself well, while the unimproved footing tips over due to excessive soil yielding beneath its corners.

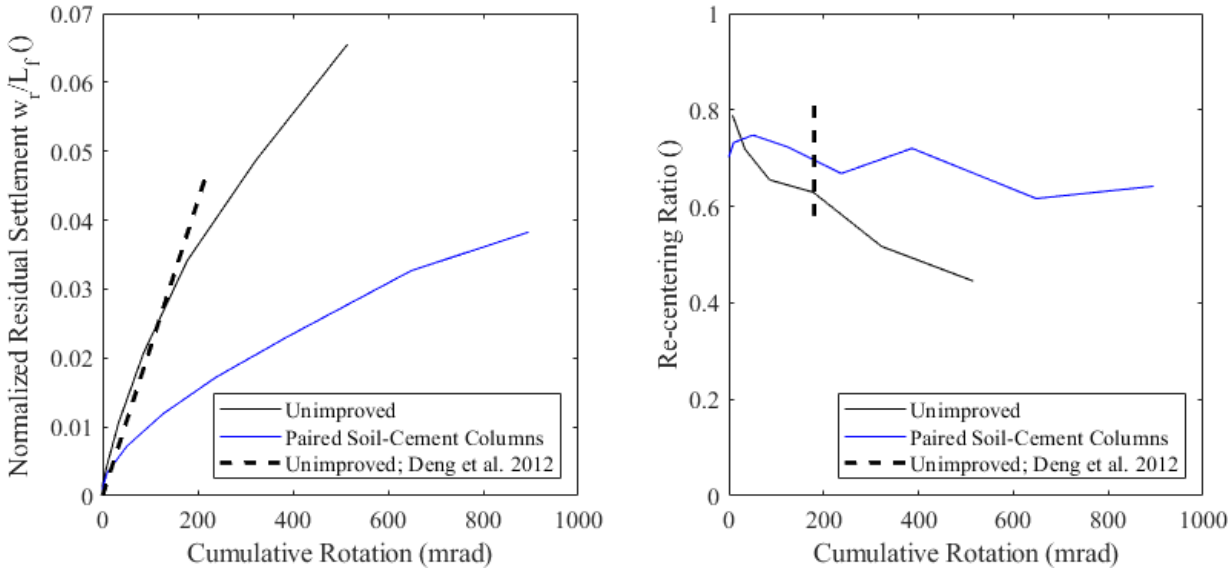

Figure 6. Rocking footing kinematics with and without ground improvement.

CONCLUSIONS

A pair of dynamic loading, rocking footing tests on unimproved sand and sand improved by soil-cement columns have been conducted in the centrifuge at UCSD. The soil-cement column mix design and strength were detailed and shown to be consistent with a case history from a sandy field site. Placement of a pair of columns at each end of the footing substantially reduced its residual settlement and preserved its re-centering ability compared to the unimproved case under a series of demanding seismic events.

ACKNOWLEDGEMENTS

The present study is funded by the Pacific Earthquake Engineering Research (PEER) Center and their support is greatly appreciated. The views are those of the authors alone.

REFERENCES

Anastasopoulos, I., Kourkoulis, R., Gelagoti, F., and Papadopoulos, E. (2012). "Rocking response of SDOF systems on shallow improved sand: An experimental study." *Soil Dynamics and Earthquake Engineering*, 40, 15-33.

Arora, S., Shao, L., and Schultz, J.M. (2012). "Wet soil mixing for bearing capacity, liquefaction mitigation, and water cutoff for scour protection for a new bridge abutment." *Grouting and Deep Mixing*, 575-584.

Deng, L., Kutter, B.L., and Kunnath, S.K. (2012). "Centrifuge modeling of bridge systems designed for rocking foundations." *Journal of Geotechnical and Geoenvironmental Engineering*, 138(3), 335–344.

Deng, L. and Kutter, B.L. (2012). "Characterization of rocking shallow foundations using centrifuge model tests." *Earthquake Engineering and Structural Dyn.*, 41(1), 1043-1060.

Gajan, S. and Kutter, B.L. (2008). "Capacity, settlement, and energy dissipation of shallow footings subjected to rocking." *Journal of Geotechnical and Geoenvironmental Engineering*, 134 (8), 1129–1141.

Gavras, A.G., Kutter, B.L., Hakhamaneshi, M., Gajan, S., Tsatsis, A., Sharma, K., Kohno, T., Deng, L., Anastasopoulos, I., and Gazetas, G. (2020). "Database of rocking shallow foundation performance: Dynamic shaking." *Earthquake Spectra*, 36 (2), 960-982.

Gazetas, G (1991). "Formulas and charts for impedances of surface and embedded foundations." Journal of Geotechnical Engineering, 117 (9), 1363-1381.

Housner, G.W. (1963). "The behavior of inverted pendulum structures during earthquakes." *Bulletin of the Seismological Society of America*, 53 (2), 403-417.

Khosravi, M., Boulanger, R.W., and Wilson, D.W. (2019). "Stress transfer from rocking shallow foundations on soil-cement reinforced clay." *Soils and Foundations*, 59 (4), 966-981.

Kutter, B.L. (1992). "Dynamic centrifuge modeling of geotechnical structures." *Transportation Research Record.* 1336.

Liu, W. and Hutchinson, T.C. (2018). "Numerical investigation of stone columns as a method for improving the performance of rocking foundation systems." *Soil Dynamics and Earthquake Engineering*, 106, 60-69.

Newgard, J.T., Hutchinson, T.C., and McCartney, J.S. (2022). "Centrifuge shake table tests on rocking footings on sand." *Proceedings of Geo-Congress 2022: Geophysical and Earthquake Engineering and Soil Dynamics*, 629-637.

Sharma, K. and Deng, L. (2020). "Field testing of rocking foundations in cohesive soil: cyclic performance footing mechanical response." *Canadian Geotech. Journal*, 57 (6), 828-839.

Veletsos, A.S. and Meek, J.W. (1974). "Dynamic Behaviour of Building-Foundation Systems." *Earthquake Engineering and Structural Dynamics*, 3, 121-138.

Zheng, Y., Fox, P.J., Shing, P.B., and McCartney, J.S. (2019). "Physical model tests on half-scale geosynthetic reinforced soil bridge abutments. I: Static loading." ASCE Journal of

Geotechnical and Geoenvironmental Engineering. 145(11), 04019094.